Bioactive Materials 29 (2023) 72–84

Contents lists available at ScienceDirect

Bioactive Materials

journal homepage: www.keaipublishing.com/en/journals/bioactive-materials

Multifunctional magnesium organic framework-based photothermal and pH dual-responsive mouthguard for caries prevention and tooth self-healing promotion

Qun Li [a,b,e], Jinbiao Liu [b], Huijie Liu [a,b,e], Yue Sun [c], Yingying Xu [a,b,e], Kexin Wang [b], Wenjing Huang [b], Lan Liao [a,d,e,**], Xiaolei Wang [b,c,*]

[a] Affiliated Stomatological Hospital, Nanchang University, Nanchang, Jiangxi, 330006, PR China
[b] National Engineering Research Center for Bioengineering Drugs and the Technologies, Institute of Translational Medicine, Nanchang University, Nanchang, Jiangxi, 330088, PR China
[c] College of Chemistry and Chemical Engineering, Nanchang University, Nanchang, Jiangxi, 330088, PR China
[d] Jinggangshan University, Ji'an, Jiangxi, 343009, PR China
[e] Key Laboratory of Oral Biomedicine, Nanchang, Jiangxi, 330006, PR China

ARTICLE INFO

Keywords:
Photothermy
pH-response
Remineralization
Caries prevention

ABSTRACT

Caries is considered to be the most prevalent non-communicable disease in humans, mainly deriving from acidogenic bacterial biofilm and resulting in the demineralization and decomposition of hard dental tissue. Herein, a composite responsive foam brace loaded with magnesium organic framework (MPC) is designed for caries prevention and tooth remineralization. MPC can intelligently release organic antibacterial molecules (gallic acid) and mineralized ions (Mg^{2+}, Ca^{2+} and PO_4^{3-}) under acidic conditions (pH < 5.5) of biofilm infection, regulating pH and killing bacteria. Additionally, due to the excellent photothermal conversion efficiency, MPC can further enhance the destruction of bacterial biofilm by inhibiting virulence genes and destroying bacterial adhesion under near-infrared light irradiation (808 nm). More importantly, MPC can not only reverse the cariogenic environment at both pH and microbial levels, but also promote self-healing of demineralized teeth in terms of both the micro-structure and mechanical properties.

1. Introduction

Dental caries caused by oral microbiome dysbiosis with the elevation of acidogenic bacteria is the most prevalent non-communicable disease worldwide [1]. The major etiological factor of caries is the bacterial biofilm [2], which adheres to dental surface, produces organic acids, forms an acidic (pH < 5.5) environment, leads to main inorganic matter of the hard tooth tissue demineralization (loss of Mg^{2+}, Ca^{2+}, PO_4^{3-}) [3] and organic matter (collagen) decomposition [4]. Without intervention, these processes will result in cavities formation, accompanied by tooth sensitivity [5] and even tooth loss eventually, which seriously affects aesthetics and quality of life [6]. At present, the major therapy measures for caries are antibacterial agents combined with artificial filling [7,8]. However, the conventional antimicrobial agents cannot effectively target the cariogenic pathogens (such as *Streptococcus mutans*, *Streptococcus sobrinus* and *Actinomyces viscosus*) in specific sites. The indiscriminate broad-spectrum sterilization easily disturbs the oral flora and even the entire human system, and increases the risk of drug resistance development [9–11]. On the other hand, dental defects filled by modern dental materials are usually susceptible to microleakage between the biological tissues at the lesion/restorative material interface, increasing the risk of adverse reactions and caries recurrence [12–15]. Based on the above discussions, a multi-functional platform should be the development direction of anti-caries: (1) Identify the microbial signals of cariogenic pathogens effectively, thereby specifically eliminating bacterial biofilm without disturbing the microbiome homeostasis and

Peer review under responsibility of KeAi Communications Co., Ltd.
* Corresponding author. National Engineering Research Center for Bioengineering Drugs and the Technologies, Institute of Translational Medicine, Nanchang University, Nanchang, Jiangxi, 330088, PR China.
** Corresponding author. Affiliated Stomatological Hospital, Nanchang University, Nanchang, Jiangxi, 330006, PR China.
E-mail addresses: Liaolan5106@ncu.edu.cn (L. Liao), wangxiaolei@ncu.edu.cn (X. Wang).

https://doi.org/10.1016/j.bioactmat.2023.06.017
Received 14 February 2023; Received in revised form 31 May 2023; Accepted 20 June 2023

surrounding mucosal tissues. (2) Reverse caries progression from bacterial biofilm and acidic niches. (3) Stabilize dental hard tissue. (4) Promote tooth self-repairing.

Recently, responsive strategies have been reported for oral health in precise sites and controlled manners. The acidic conditions displayed by cariogenic pathogens can act as endogenous stimuli to enable responsive biomaterials to function at target sites. For example, Huang et al. [16] proposed a multidrug delivery system (PMs@NaF-SAP) for caries treatment that responded to low pH signals. As a natural gallnut extract, gallic acid exhibits positive applications in the prevention of caries with good anti-inflammatory, anti-bacterial and bio-compatible properties [17,18]. Metal-organic framework (MOF) is an attractive nano-platform for controlled drug delivery with the unique structure which collapses under acidic conditions [19,20]. By combining MOF with gallic acid, intelligent release of gallic acid in cariogenic environment (low pH) can be achieved, which may provide a new strategy for caries treatment. On the other hand, as an exogenous stimulus, light source modulation has certain advantages due to its non-operational, non-invasive and high spatio-temporal accuracy [21,22]. However, the harmful effects of short-wavelength light sources (ultraviolet light and blue light) to humans, such as oxidative damage to the skin [23] and photochemical damage to the retina [24], have been widely reported. Therefore, photothermal therapy (PTT) based on healthy long-wavelength (near infrared, NIR) light has received increasing attention in the design of antibacterial system. Among them, poly-dopamine (PDA), as a photothermal agent, has a good photothermal conversion ability, which can further enhance the antibacterial activity of the above system under NIR irradiation.

Based on the above discussion, a pH and NIR dual-responsive composite system for caries treatment was proposed, combining the both advantages of intelligent pathogenic microbial response and highly accurate control as described above. In addition, the strategy aims to achieve a multifunctional and comprehensive anti-caries effect while being convenient to use. As shown in Fig. 1a, gallic acid, a natural gallnut component, was used as an organometallic framework to form magnesium-organic framework (Mg-MOF) [25]. Then PDA with outstanding photothermal conversion efficiency was wrapped on the Mg-MOF [26]. Finally, calcium phosphate (CaP) was loaded on the surface of Mg-MOF@PDA by biomimetic mineralization to form composite nanomaterial Mg-MOF@PDA@CaP (MPC). To facilitate the application of this system, MPC-CB foam braces were formed by loading with the foaming agent (cocamidopropyl betaine, Fig. 1b). Accordingly, as shown in Fig. 1c, the following null hypotheses were tested: 1) The pathophysiological pH fluctuations in the oral microenvironment caused by caries could trigger this intelligent nanosystem. Under acidic conditions generated by biofilm infection, the CaP coating of MPC degraded and released Ca^{2+} and PO_4^{3-}, followed by the release of Mg^{2+} and naturally active antimicrobial molecules (gallic acid) from the collapsed organic framework; 2) MPC could exhibit excellent biofilm destruction under NIR irradiation; 3) The degradation of coating and frame could ameliorate the low pH situation of the lesion site and reverse the carious environment; 4) Gallic acid and PDA had good affinity for inorganic components (calcium and phosphorus) and organic component (collagen) in tooth tissue, which could effectively stabilize tooth hard tissue [27,28]. Furthermore, the released Ca^{2+}, PO_4^{3-} and Mg^{2+} could promote the self-repair of teeth, and then restore the mechanical properties [26–31].

2. Materials and methods

2.1. Materials

Magnesium chloride ($MgCl_2$), gallic acid, potassium hydroxide (KOH), dopamine hydrochloride, Tris (hydroxymethyl) aminomethane hydrochloride (Tris-HCl), ethylene diamine tetraacetic acid (EDTA), potassium chloride (KCl), L-ascorbic acid, sodium hydroxide (NaOH), glycine (Gly) and calconcarboxylic acid were obtained from Aladdin Bio-chem Technology (Shanghai, China). Cell counting kit-8 (CCK-8), collagen type I (Col-I) and adenosine triphosphate (ATP) assay kit were purchased from Solarbio (Beijing, China). Alkaline phosphatase (ALP) kit, malachite green phosphate detection kit, alizarin red staining kit, live and dead bacterial staining kit were obtained from Beyotime Biotechnology Co. (Jiangsu, China).

2.2. Fabrication of MPC

Firstly, Mg-MOF was synthesized by solvothermal method [25]. Specifically, 1 g $MgCl_2$, 3.8 g gallic acid and 50 mL water were mixed in

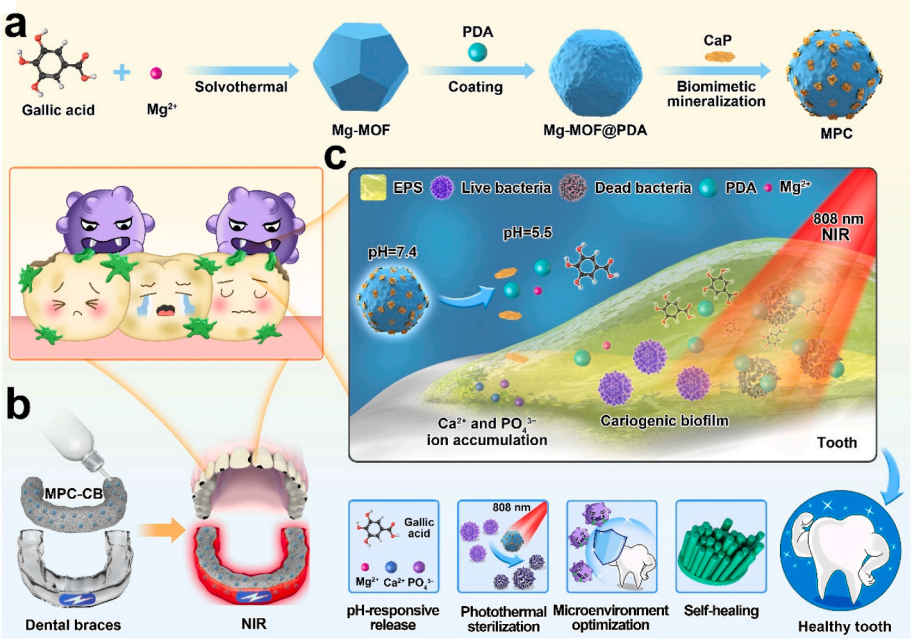

Fig. 1. Schematic illustration of construction of MPC and working principle. (a) The construction of MPC. (b) The usage of MPC. (c) Photothermal and pH dual-responsive MPC for localized biofilm disruption, oral microenvironment optimization and tooth hard tissue self-healing.

a beaker, and then the pH of the suspension was adjusted to 8 with KOH aqueous solution (10 M). After stirring for 15 min, the orange solution was poured into a teflon autoclave (100 mL) and kept at 140 °C for 24 h. Subsequently, the reaction mixture was centrifuged at 10000 rpm for 10 min and washed several times with deionized water and anhydrous ethanol to obtain Mg-MOF. Secondly, the above products and dopamine hydrochloride were added in the ratio of 1:3 (w/w) to Tris-HCl (pH = 8.5) and stirred for 12 h, and then the PDA was concentrated on the surface of the Mg-MOF to form a coating. Mg-MOF@PDA was obtained after centrifugation at 10000 rpm, washing and lyophilization. Finally, the nanoparticles were dispersed in simulated body fluid (SBF) at a concentration of 5 mg mL^{-1}. The reaction was stirred at 37 °C for 12 h to induce a CaP coating on the surface of Mg-MOF@PDA particles to obtain MPC.

2.3. Characterization

The morphology and chemical composition of samples were characterized by scanning electron microscopy (SEM, Zeiss/Sigma 300, Germany). Then morphology and element mapping of the MPC were also observed by transmission electron microscopy (TEM, JEM-100SX, Japan) equipped with energy dispersive spectrometry (EDS). The particle sizes of samples were measured using dynamic light scattering (DLS, Zetasizer Nano ZS90, Malvern Instruments, Malvern, UK), and fourier transform infrared (FT-IR) spectra were collected on a FT-IR spectroscopy (Nicolet, Nicolet 5700, USA). The crystalline structure and characterization of the samples were analyzed by X-ray diffraction (XRD, BrukerD8A A25 X).

2.4. Photothermal effect of MPC

Mg-MOF (400 μg mL^{-1}) as well as MPC (400 μg mL^{-1}) were used as experimental groups and phosphate buffered saline (PBS) was used as the Control group to be exposed to 808 nm NIR (1.5 W cm^{-2}). The real-time temperature changes of PBS, Mg-MOF and MPC were recorded with an infrared thermal imaging camera (E54, Teledyneflir Company, China).

2.5. In vitro pH-responsiveness

MPC was placed in an aqueous solution with pH = 5.5 for different times, and then its morphology was observed by the SEM. The aqueous solution was adjusted to different pH values (pH = 4.5, 5.5, 6.5, 7.5, 8.5), and the MPC was configured as a mixed solution of different pH values (1 mg mL^{-1}). After 30 min, the supernatant was collected by centrifugation at 10000 rpm. The calconcarboxylic acid was used to detect the released Ca^{2+}, and the absorbance value of each group was recorded by an ultraviolet–visible (UV–vis) spectrophotometer at the wavelength of 620 nm. The contents of PO_4^{3-} released from different pH values were detected by malachite green phosphate detection kit, and the released contents of Mg^{2+} were detected by inductive coupled plasma emission spectrometer (ICP). The amount of released gallic acid could be directly detected by testing the increase in absorbance intensity at 260 nm. Specifically, 1 mg of MPC was added to 10 mL of aqueous solution at different pH values, and the absorption spectra of gallic acid released at different times were recorded by UV–vis spectrophotometer.

2.6. In vitro bacterial microenvironment regulation

In order to verify the pH value changes of caries-driven bacteria with time, we selected three representative bacteria (*Streptococcus mutans*, *Streptococcus sobrinus* and *Actinomyces viscosus*) and mixed bacteria solution (containing three representative cariogenic bacteria, including *Streptococcus mutans*, *Streptococcus sobrinus* and *Actinomyces viscosus*, and the concentration of the three bacteria was equal, with a total concentration of 1×10^7 CFU mL^{-1}) to be cultured in brain heart infusion (BHI) medium (5 mL) with 1% sucrose for 48 h, and then the pH values were detected. In addition, the bacteria suspensions co-cultured with MPC (400 μg mL^{-1}) and NIR irradiation (1.5 W cm^{-2}, 5 min) were used as the experimental group. Subsequently, the pH values at different times were recorded and compared with those of untreated bacterial suspensions. Four typical oral bacteria (*Streptococcus mutans*, *Streptococcus sobrinus*, *Actinomyces viscosus* and *Candida albicans*) in the logarithmic growth stage co-cultured with MPC as the experimental groups and the optical density (OD) values of the suspension at 600 nm were recorded. The changes of OD values were recorded as the formula:

$$\Delta OD = OD_{control} - OD_{experiment} \quad \text{Equation (1)}$$

where $OD_{control}$ and $OD_{expriment}$ represented the OD values in the Control group and the experimental groups, respectively. In the control group and the experimental group, the bacteria grew naturally in the medium at 37 °C and co-cultured with the MPC, respectively.

2.7. In vitro antibacterial activity

Staphylococcus aureus (*S. aureus*) and *Escherichia coli* (*E. coli*) were cultured in Luria-Bertani broth, while *Streptococcus mutans* (*S. mutans*), *Streptococcus sobrinus* (*S. sobrinus*), *Actinomyces viscosus* (*A. viscosus*) were cultured in a BHI broth. All of them were adjusted to an appropriate concentration (1×10^7 CFU mL^{-1}) to conduct antibacterial experiments. Samples were added to 5 mL of medium containing bacterial solution (100 μL) and incubated for 5 min with/without NIR irradiation. The bacterial suspension was diluted 1×10^5-fold with PBS, and then 50 μL of the dilution was co-cultured on plate at 37 °C for 1−2 days. The antibacterial properties (R) of different samples were analyzed by plate counting method based on the following formula:

$$R\ (\%) = (N_c - N) / N_c \times 100\% \quad \text{Equation (2)}$$

where Nc represented the number of bacterial colonies in the Control group and N represented the number of bacteria in the experimental groups. The morphologies of all bacteria treated differently were observed by SEM.

2.8. Preparation of teeth slices

The extracted human molars with complete surfaces were selected and cleaned. The crown was dissected into 1 mm thick slices along the crown-root axis by a hard tissue slicing machine (E300CP, EXAKT, Germany), and then polished by different types of sandpaper in turn. Finally, the 4 mm × 5 mm teeth slices were obtained and classified as enamel slices and dentin slices, respectively.

2.9. Destruction of biofilm in vitro

Enamel slices were selected and placed in the 12-well plates. Subsequently, the enamel slices were immersed in 2 mL bacterial suspension of *S. mutans*. Biofilms were formed by anaerobic incubation at 37 °C for 3 days. To detect the inhibition and destruction of biofilm formation by MPC, enamel slices were treated with different samples during anaerobic culture and after biofilm formation, respectively. Subsequently, biofilms on the enamel surface were collected by vigorous scour and oscillation. Plate counting method was used to analyze the anti-biofilm ratio by comparing the colony number (N) of the experimental group and the colony number (Nc) of the Control group based on Equation (2). Meanwhile, biofilms were collected, centrifuged and lyophilized, then weighed and recorded. The biofilms treated with MPC were fixed with glutaraldehyde, stained with 0.1% crystal violet, followed by ethyl alcohol to dissolve the blue-violet crystals, and the related OD values at 600 nm were determined. In addition, the morphologies of the *S. mutans* biofilms adhered to the tooth surface were observed by SEM. Live and dead staining assays of biofilms were conducted as well. The biofilms on

the coverslip were cultured for 3 days and stained with 10 μg mL^{-1} NucView Green Live (live bacteria) and propidium iodide (PI, dead bacteria) dyes, respectively, and then imaged with an inverted fluorescence microscope (IX 83, Olympus, Japan).

2.10. Antibacterial mechanisms

Biofilms co-cultured with different samples were collected after centrifugation at 11500 rpm for 15 min, and subsequently the 3% EDTA was added, and then the supernatant was obtained after centrifugation and filtration with a pore size of 0.45 μm membrane. 98% sulfuric acid and phenol were added to the above liquid, and OD values of 400 nm were recorded 20 min later to measure the contents of water insoluble polysaccharide in the biofilms. Additionally, the intracellular ATP production in *S. mutans* was also evaluated. The biofilm solutions with different treatments were collected, and the amount of ATP was determined using an ATP assay kit. The fluorescence intensity was evaluated using a microporous plate luminescence detector (Centro LB 960, Create Technology Co., Beijing). Quantitative reverse transcription-PCR (qRT-PCR) was used to detect bacterial biofilm adhesion and cariogenicity at the genetic level. *S. mutans*-specific targeted caries causing genes (gbpD, gtfC) and genes related to density sensing adaptive regulatory system (comE and comD) were analyzed. The biofilms on enamel were treated and collected as described above. The primers were synthesized by Wuhan Servicebio Technology CO., LTD and relevant sequences were listed in Table S1.

2.11. Preparation of the remineralization samples

To both simulate early caries lesions and remove the prism-less enamel of the outermost tooth surface, the enamel samples were etched with phosphoric acid (H_3PO_4, 37 wt%) for 5 min. The dentin slices were etched for 1 min as described above for the follow-up experiment. Then the acid-etched samples were immersed in artificial saliva at 37 °C for 5 days. During the treatment, they were soaked in MPC solution for 15 min twice a day as the experimental group. After incubation, the repaired enamel and dentin slices were sonicated in water for 5 min, rinsed with water, and air-dried before remineralization examination.

2.12. Remineralization examination assay

The as-prepared samples were measured by SEM and XRD (X-ray diffraction, X'Pert PRO MPD) with a sampling step of 5° min^{-1} in the 2θ range from 10° to 60°. Nanoindentation testing was carried out in a nanoindenter (NanoTest Vantage, MML, UK), and then the nanohardness and elastic modulus were obtained by calculating the force-displacement curves. Subsequently, the self-assembled liquor containing 50 mM Gly and 200 mM KCl was prepared, and the pH was adjusted to 9.2 with 1 M NaOH. The Col-I solution was mixed with self-assembly solution to get 50 μg mL^{-1} collagen solution. Collagen-loaded nickel grids were prepared and immersed in artificial saliva for 5 days. During this period, the experimental group was treated with MPC twice a day for 15 min each time for SEM observation. In order to observe the morphology of *in situ* collagen fibers, the dentin was etched for a short time to expose smaller and shallower dentin tubules, and then treated with MPC for 30 min and immersed in artificial saliva for 24 h in succession for the experimental group, which was prepared for SEM observation.

2.13. Demineralization inhibition assay

In order to simulate the demineralization environment, artificial demineralization solution was prepared according to the principle of chemical caries. Specifically, 0.26 g calcium nitrate, 0.15 g potassium dihydrogen phosphate, and 0.15 g glacial acetic acid were added to 500 mL pure water solution, and then the pH was adjusted to 4.5 with potassium hydroxide. The enamel and dentin slices were immersed in the demineralized solution for 12 h. During this period, MPC (experimental group) or artificial saliva treatment (DF group) was conducted every hour. After incubation, the slices were washed as before and prepared for SEM, XRD and nanoindentation analysis.

2.14. pH regulation

An enamel slice was immersed in the demineralized solution and the surface pH was detected as the initial pH condition. Then the surface pH of the enamel was measured after being immersed in artificial saliva, Mg-MOF and MPC for 15 min, respectively.

2.15. Hemolysis assay

3 mL blood was obtained from Sprague-Dawley (SD) rats and centrifuged at 1500 rpm for 15 min to get rat red blood cells (RBCs). Subsequently, RBCs were diluted with 0.9% sodium chloride (NaCl) solution to get RBCs suspension. After that, 1.1 mL of 0.9% NaCl solution, 1.1 mL of deionized water, and 1.1 mL of different concentrations of MPC solutions were added as negative control group, positive control group and experimental group, respectively. The supernatant was obtained by centrifugation at 1500 rpm for 15 min after water bath at 37 °C for 1 h. The OD values at 540 nm were measured by the spectrophotometer and the hemolysis ratio (HR) was calculated according to the following formula:

$$\mathrm{HR}\ (\%) = \frac{\mathrm{OD}_{\text{experimental group}} - \mathrm{OD}_{\text{negative group}}}{\mathrm{OD}_{\text{positive group}} - \mathrm{OD}_{\text{negative group}}} \times 100\% \qquad \text{Equation (3)}$$

2.16. Cytotoxicity experiment

Human normal oral keratinocytes (HOK) cells, mouse fibroblasts (L929) cells and mouse pre-osteoblasts (MC3T3-E1) cells were selected for biosafety experiments. The cells were seeded in 96-well plates and cultured with different concentrations of MPC. The cells co-cultured for 1, 2 and 3 days were detected by CCK-8 kit. The OD values at 450 nm were measured by the spectrophotometer and calculated as the following formula:

$$\text{Cell viability}\ (\%) = \mathrm{OD}_{\text{test}}\ /\mathrm{OD}_{\text{control}} \qquad \text{Equation (4)}$$

For live and dead cell staining assay, the cells were seeded in 6-well plates with different samples impregnation solutions for 24 h and then stained with Calcein-AM/PI. After incubation for 15 min at 37 °C in the dark, live cells were stained green, while dead cells exhibited red fluorescence, both of which were observed by inverted fluorescence microscope.

2.17. Osteogenesis potential exploration

MC3T3-E1 cells were cultivated in 6-well plates and co-cultured with osteoinductive culture media containing 100 nM dexamethasone, 50 μg mL^{-1} ascorbic acid, 100 mM β-glycerophosphate and 400 μg mL^{-1} MPC. After 14 days of cultivation, the cell differentiation was evaluated by detecting ALP in the cell lysates using an ALP staining kit. Alizarin red staining was also conducted to identify the calcium deposition. The cells in different groups were fixed with 4% paraformaldehyde for 15 min and stained with 1% alizarin red solution for 30 min. The stained cells were observed under an optical microscope and calculated by Image J.

2.18. Animal experiment

All animal procedures were performed with the Guidelines for the Care and Use of Laboratory Animals of Nanchang University in China and approved by the Animal Ethics Committee of Nanchang University

(Nanchang, China, SYXK2015-0003). Female SD rats (14-day-old) were obtained from Jiangxi University of Chinese Medicine. The rats were infected with *S. mutans* (2×10^9 CFU mL^{-1}) for 5 consecutive days as previous research (Each rat was injected with 0.2 mL of bacterial solution, fasted within 1 h after swabbed the bacterial solution, and repeated twice a day) [7]. After 5 days, in the experimental groups, the teeth of rats were coated with MPC-CB and then removed after 10 min of NIR illumination, which was repeated once a day. During the treatment, these animals were fed with the cariogenic Keyes 2000 Diet (Jiangsu Syony Bioengineering Co., LTD, China) and 5% sucrose water. After 40 days, the whole blood of the rats was collected for routine blood analysis, and the plasma was collected for blood biochemical index detection. In addition, heart, liver, spleen, lung, kidney, tongue mucosa and gingival tissues around the teeth were collected for biosafety analysis.

2.19. Caries prevention in vivo

Before the rats were sacrificed, the biofilms on the surface of the first molar were scraped with sterile bamboo stick, diluted with PBS, inoculated on the selective medium of mitis salivarius agar plus bacitracin (MSB), and the formation and number of colonies were observed. After the rats were sacrificed, the maxilla and mandible were taken out and stained with 2% basic magenta for 3 min, then washed with water, and the images were recorded. The size of staining area was analyzed to evaluate the effect of biofilm disruption. For dental caries, the jaws of rats were stained with 0.4% murexide for 24 h, and images of the maxilla and mandible were recorded. Caries scoring was recorded according to the Keyes' system.

2.20. Statistical analysis

All data obtained were expressed as mean ± standard deviation (SD). Statistical analyses were performed using GraphPad Prism (GraphPad Software, Inc., San Diego, CA), one-way analysis of variance (ANOVA) and *t*-test were used for statistical analysis. The probability value (p value) < 0.05 was considered statistically significant.

3. Result and discussion

3.1. Preparation and characterization of MPC

The synthesis process of MPC was shown in Fig. 1a. Firstly, Mg-MOF was synthesized by hydrothermal method with $MgCl_2$ and gallic acid at pH = 12, and PDA coating was naturally deposited on the surface of Mg-MOF to form Mg-MOF@PDA. Finally, CaP coating was constructed on the surface of Mg-MOF@PDA by biomimetic mineralization to form

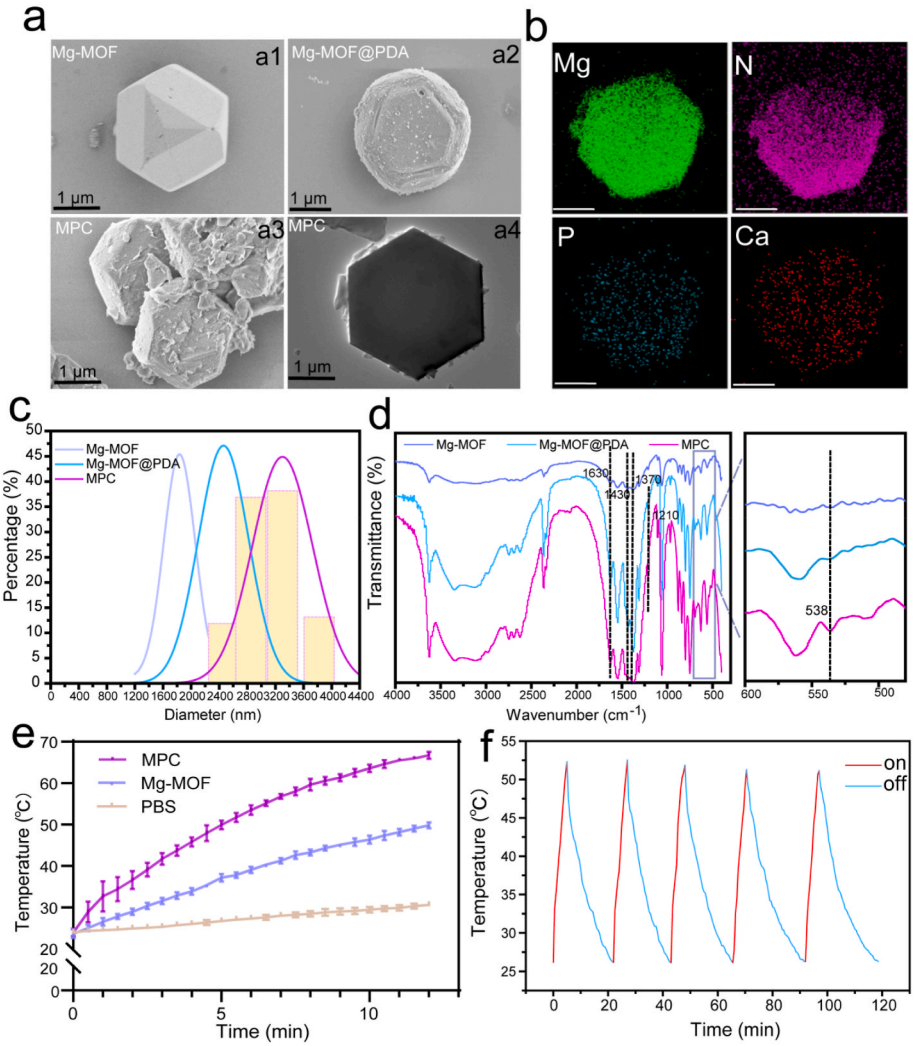

Fig. 2. (a) SEM images of Mg-MOF (a1), Mg-MOF@PDA (a2), MPC (a3) and TEM image of MPC (a4). (b) Elements distribution of MPC. (Scale bar = 1 μm). (c) Size distribution of Mg-MOF, Mg-MOF@PDA and MPC. (d) FT-IR spectra and the magnified view (right) of Mg-MOF, Mg-MOF@PDA and MPC. (e) Temperature elevation curves of PBS, Mg-MOF and MPC under NIR irradiation (1.5 W cm^{-2}). (f) Temperature changes of MPC after five NIR on/off cycles. Data are means ± SD (n = 3).

MPC [32]. Next, the morphologies of the synthesized products were observed. Mg-MOF showed a regular polyhedral structure with the size of approximately 1–3 μm (Fig. 2a1). Subsequently, PDA was wrapped uniformly on the polyhedral surface in a granular structure to form Mg-MOF@PDA (Fig. 2a2). The surface of the MPC exhibited the accumulation of sheet structures (Fig. 2a3 and Fig. 2a4). The energy spectrum (Fig. 2b and Fig. S1) displayed the distribution of four elements (Mg, N, Ca, P). Particle size analysis showed that the size of modified Mg-MOF increased (Fig. 2c, Fig. S2 and Fig. S3). In addition, FT-IR spectra (Fig. 2d) showed C═O at 1630 cm^{-1}, C═C and benzene ring skeleton vibration at 1430 cm^{-1} and 1370 cm^{-1}. There was C–N absorption peak at 1210 cm^{-1} in Mg-MOF@PDA, and the slight blue shift was considered to be the result from non-covalent binding of PDA on the Mg-MOF surface by π−π packing. The blue shift of peak C═O in MPC was considered to the result from p−π conjugation of PDA chelating Ca^{2+}. There was P–O bending vibration peak at 538 cm^{-1} in MPC. The MPC exhibited multi-layer structures maintaining the crystal structure integrity of the pristine Mg-MOF as characterized by X-ray diffraction (Fig. S4). All of the above proved the successful synthesis of Mg-MOF, Mg-MOF@PDA and MPC [32].

Next, we investigated the photothermal conversion performance of MPC. As shown in Fig. 2e and Fig. S5, the temperature of the MPC solution could be raised to approximately 48 °C after 5 min 808 nm NIR irradiation (1.5 W cm^{-2}), which showed the most superior photothermal conversion performance compared with PBS and Mg-MOF solution. In addition, after five temperature-cooling switch cycle experiments, the results showed that MPC could still rise to approximately 48 °C, indicating that it had a relatively stable photothermal conversion performance (Fig. 2f), which provided the basis for MPC to perform antibacterial efficacy on demand *via* NIR irradiation.

3.2. pH responsiveness

Low pH (pH < 5.5) niches demineralize the structure of the tooth hard tissue and lead to carious lesion formation [2–4]. Thus, local caries lesions targeting can be achieved through this distinguishing feature —— pH signal responsiveness. In order to test the pH responsiveness of MPC, it was placed in aqueous solution at pH = 5.5 for different times, and the morphology was observed by SEM. It was shown that the CaP layer decomposed and three-dimensional framework structure of Mg-MOF also broke and collapsed over time (Fig. 3a). The contents of Ca^{2+} in the supernatant of MPC solution (10 mg L^{-1}) were detected by calcium indicator at different pH values after 30 min. Fig. 3b showed that the CaP layer on the surface of MPC decomposed in a short time under acidic environment, and the content of Ca^{2+} released was significantly higher than that under high pH environment. The contents

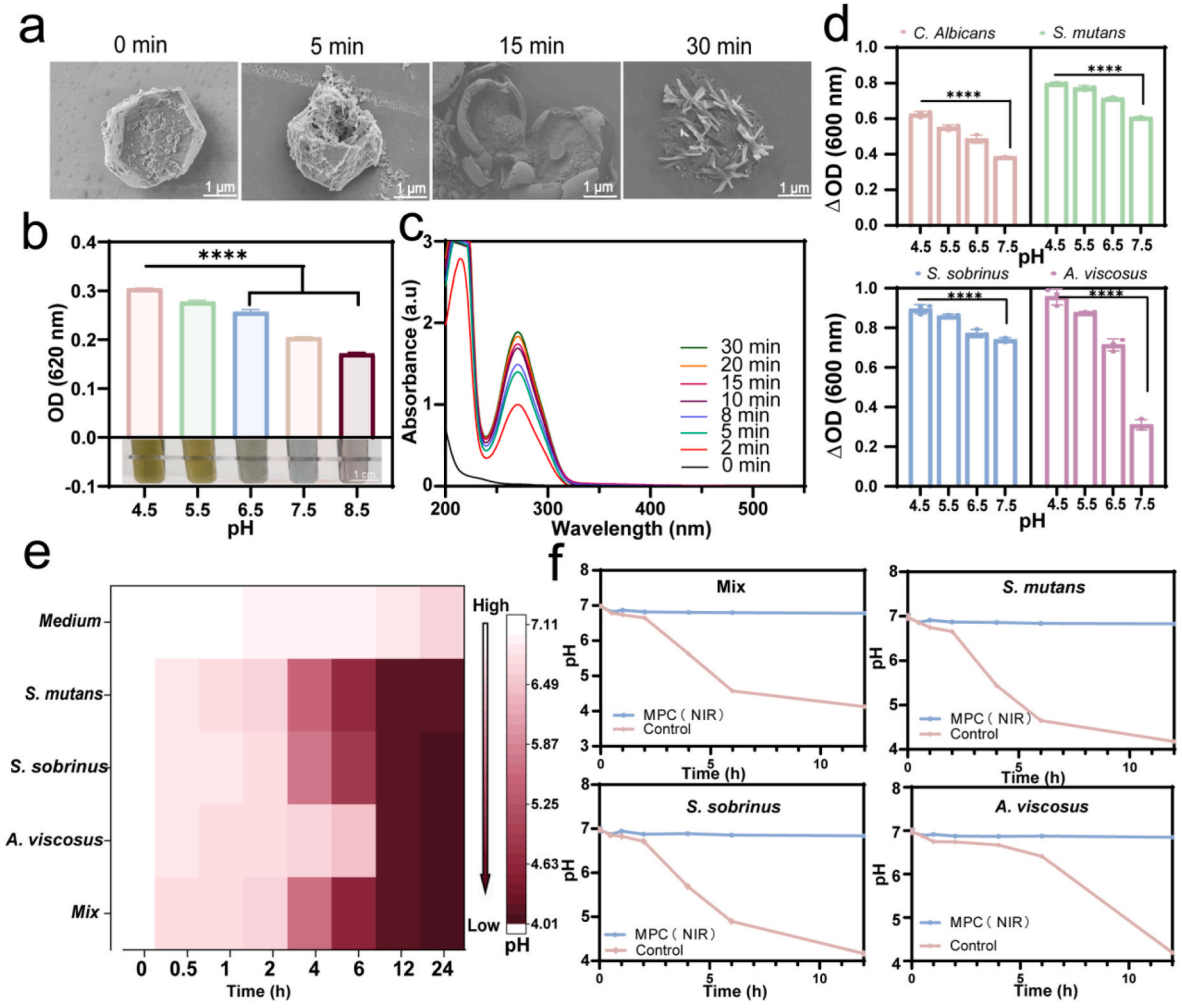

Fig. 3. pH responsiveness of MPC. (a) SEM morphologies of MPC at different times (pH = 5.5). (b) Ca^{2+} contents released from MPC at different pH values after 30 min. (c) The UV–vis absorption spectra of MPC at different times determined by the released gallic acid (pH = 5.5). (d) OD value changes of *C. albicans*, *S. mutans*, *S. sobrinus* and *A. viscosus* after co-culture with MPC at different pH values. (e) pH changes of three representative cariogenic bacteria as a function of time (*S. mutans*, *S. sobrinus*, *A. viscosus* and mixed flora). (f) pH changes of different bacterial suspensions after co-culture with MPC for different times. Data are means ± SD. (n = 3). ****$p < 0.0001$.

of PO_4^{3-} and Mg^{2+} released from different pH values were detected, both of which exhibited similar tendency as Ca^{2+} release (Fig. S6 and Fig. S7). Meanwhile, the absorbance of MPC was recorded by a UV–vis spectrophotometer, and the peak value located at 260 nm was determined by gallic acid released from collapsed MPC. The release amount of gallic acid gradually increased over time at pH = 5.5 (Fig. 3c). In addition, it was found that the lower pH value, the higher release amount of gallic acid by comparing the peak values at different pH values (Fig. S8).

In addition, the bacteria were co-cultured with MPC at different pH values, and the OD values at 600 nm were recorded, which was used to

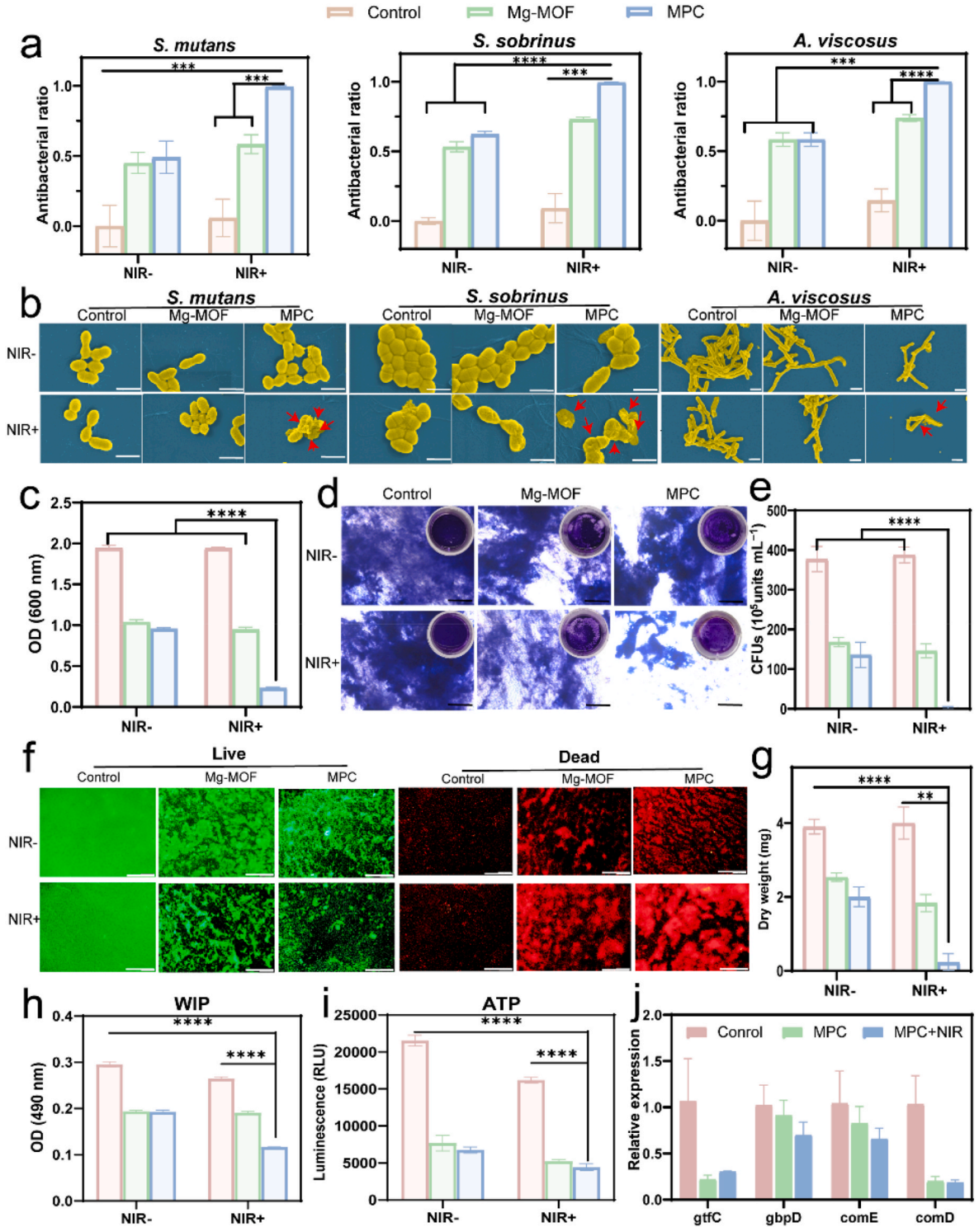

Fig. 4. *In vitro* antibacterial activity of MPC. Antibacterial ratios (a) and SEM images (b) of Mg-MOF and MPC against *S. mutans, S. sobrinus* as well as *A. viscosus* with/without NIR irradiation. (Scale bar = 1 μm). The biofilm viabilities (c) and crystal violet staining images (d) after different treatments. (Scale bar = 200 μm). (e) Viabilities of bacterial biofilm after different treatments. (f) Fluorescence images of *S. mutans* with different treatments, live cells were stained green and dead cells were stained red. (Scale bar = 50 μm). (g) The mass of biofilms with different treatments. (h) The OD values of water insoluble polysaccharide in bacterial biofilms and luminescence intensions of ATP (i) of bacterial biofilms with different treatments. (j) Relative expressions of genes related to *S. mutans* treated with different treatments. Data are means ± SD. (n = 3). $^{**}p < 0.01$, $^{***}p < 0.001$, $^{****}p < 0.0001$.

monitor bacterial growth and viability. As shown in Fig. 3d, after co-culture with MPC, the OD values of the four kinds of common oral pathogens (*C. albicans, S. mutans, S. sobrinus* and *A. viscosus*) changed, and the lower the pH values of the culture condition, the higher the ΔOD values of the bacteria. This indicated that MPC exhibited better antibacterial capability under acidic conditions, which was mainly attributed to the improved release of the antibacterial active molecule (gallic acid) at lower pH value [33]. To develop the pH response strategy for eliminating cariogenic bacteria, the relationship between different cariogenic bacteria and pH values needed to be investigated. Therefore, the acid-producing ability of three representative bacteria (*S. mutans*, *S. sobrinus* and *A. viscosus*) was explored. As shown in Fig. 3e, the pH values of different bacterial suspensions (*S. mutans*, *S. sobrinus*, *A. viscosus* and the mixed flora) were decreased continuously and ultimately reached approximately 4 after 12 h in the presence of 1% sucrose, which demonstrated the acid-producing and acid-tolerant ability of the three representative cariogenic bacteria. Furthermore, the acidic niches (pH < 5.5) will lead to tooth demineralization and progression of dental caries, resulting in cavity defects [2]. Fortunately, the pH values of the above bacterial suspensions were relatively stable for a long time after co-culture with MPC followed by 5 min NIR irradiation (Fig. 3f). In order to further simulate the oral cariogenic environment, the enamel slices were soaked in demineralized solution for 1 h and then placed in different solutions for 15 min, and the pH values of the enamel slices' surface were detected. As shown in Fig. S9, the pH of tooth surface was reversed to neutral after immersion in MPC solution. These experiments demonstrated that MPC could respond to the changes of pathological microenvironment (low pH) to achieve precisely targeted therapy, effectively interrupt the caries progression and reverse the cariogenic environment.

3.3. Antibacterial efficiency

When cariogenic bacteria become the dominant bacterial community in oral cavity, it will lead to the imbalance of oral microecological environment, the decrease of pH value and the demineralization of tooth hard tissue [4]. Therefore, how to effectively inhibit and destroy the growth and reproduction of cariogenic bacteria is the focus of oral multifunctional nursing materials. Firstly, *S. mutans*, *S. sobrinus*, *A. viscosus*, as well as gram-negative bacteria (*E. coli*) and gram-positive representative bacteria (*S. aureus*) were selected to carry out relevant experiments. Fig. 4a and Fig. S10−12 showed that MPC exhibited excellent antibacterial performance after co-culture with the above five bacteria, and its antibacterial ratios increased to nearly 100% after regulation by NIR irradiation. The SEM images of bacteria after different treatments were observed. It could be seen in Fig. 4b and Fig. S13 that the cell membrane of bacteria in MPC + NIR group crumpled and ruptured (red arrow), which was related to the excellent photothermal properties and antibacterial effects of MPC. Since the flagellar structure of *A. viscosus* facilitated the adhesion of cariogenic bacteria to the tooth surface [34], TEM was used to observe the morphology of the *A. viscosus* (Fig. S14). No flagellum (white arrow) was observed after being treated with Mg-MOF and MPC, which might be related to the fact that the released gallic acid could inhibit the bacterial adhesion to some extent. In addition, bacterial rupture was visible in the MPC group (red arrow). Furthermore, a series of experiments were conducted to explore the influence of MPC on the biofilms. After 3 days of bacterial culture of *S. mutans*, a single bacterial biofilm was formed. Crystal violet was used to stain the biofilms with different treatments. OD values and images showed that MPC could damage the biofilm structure to a large extent under NIR irradiation (Fig. 4c–d). Plate counting of bacterial biofilms also showed the same result (Fig. 4e). In order to further observe the destruction of biofilms intuitively, the live and dead staining experiment was also conducted to observe the bacteria in the collected biofilms, in which the live bacteria showed green fluorescence while the dead bacteria showed red fluorescence. Fig. 4f showed that the dead bacteria accounted for a large proportion in the biofilms of MPC + NIR group. Meanwhile, the weight and the SEM images of biofilms on enamel slices also proved that MPC + NIR could almost completely inhibit the formation of biofilm (Fig. 4g and Fig. S15), which could be further indicated by the crystal violet staining analysis (Fig. S16).

Finally, we further explored the antibacterial mechanism of MPC with NIR irradiation. The amounts of O-Nitrobenzene β-D-galactoside (ONPG) were detected to measure the bacterial membrane permeability. In general, the damage to the bacterial membrane was proportional to the permeability of ONPG in bacteria [35]. MPC with NIR resulted in a noticeable increase in the hydrolysis of ONPG (Fig. S17). Bacterial biofilms are composed of bacteria and bacterial extracellular polysaccharides [36], among which extracellular water insoluble polysaccharide is a virulence factor of cariogenic bacteria and promotes adhesion for bacterial biofilms [37]. Therefore, we collected water insoluble polysaccharide from biofilms and detected its content by sulfuric acid-phenol method. As shown in Fig. 4h, MPC + NIR group could effectively remove water insoluble polysaccharide (WIP) compared with the Control group. Furthermore, MPC could reduce ATP in *S. mutans* biofilms effectively with NIR irradiation (Fig. 4i), which revealed the disruption of energy supply and metabolic processes in *S. mutans* biofilms. qRT-PCR was performed to evaluate the expression of genes associated with biofilm formation (gtfC and gbpD) and the quorum sensing system (comD and comE) of *S. mutans* UA159 treated with MPC. As shown in Fig. 4j, MPC could dramatically downregulate the expression of the above virulence genes regardless of NIR usage. The above experiments all proved that MPC combined with NIR had good antibacterial effect, as well as inhibitory effect on both the virulence genes expression and bacterial adhesion.

3.4. Mineralization promotion and demineralization inhibition

Once the hard tissue of teeth is damaged, it cannot be repaired spontaneously. Therefore, it is necessary to inhibit tooth demineralization and promote tooth mineralization. Firstly, the morphology of tooth enamel was observed to analyze the remineralization capacity (Fig. 5a, top). The results showed that the uneroded enamel had flaky and random mineral deposits on their surfaces after being soaked in saliva for 7 days. Meanwhile, the enamel soaked in saliva after being eroded with 37% H_3PO_4 had similar deposits, but the surface was rough and porous, indicating that saliva could not recover the enamel tissue destroyed by the acid etching agent. By comparison, dense rod-like structure was observed on the enamel surface after MPC treatment, which demonstrated the enamel remineralization ability of MPC. In addition, the same methods were conducted to the dentin slices. As shown in Fig. 5a, disorderly mineral precipitation was found around the dentin tubules in the Control group, while disorderly mineral accumulation was also found around the dentin tubules in the acid etching group. However, the exposed collagen fibrils in dentin tubules were visible, and it was this exposure that easily led to dentin sensitivity, such as cold and heat sensitivity pain. For the MPC group, minerals were deposited in tubules, which obscured collagen fibrils. The tubules were nearly completely occluded by blocked structures and needle-like crystals. Mineral growth around the tubule also confirms the remineralization of MPC. The hard tissue of teeth is an organic-inorganic complex of ordered nanoscale hydroxyapatite and collagen matrix [38], and the small amount of collagen plays a crucial role in the regulation of mineralization [39]. In order to explore the effect of materials on collagen, Col-I was placed in different solutions and the morphology was recorded by SEM. Fig. S18 and Fig. S19 showed significant mineralization on collagen fibers with MPC in vitro and *in situ*, respectively. It was considered to be related to the high affinity of PDA and gallic acid for collagen, which reduced the interfacial energy between collagen surface and minerals [27,28]. Further assessments were performed to confirm the demineralization inhibition of MPC. Specifically, the enamel slices were immersed in the demineralized solution, and the experimental

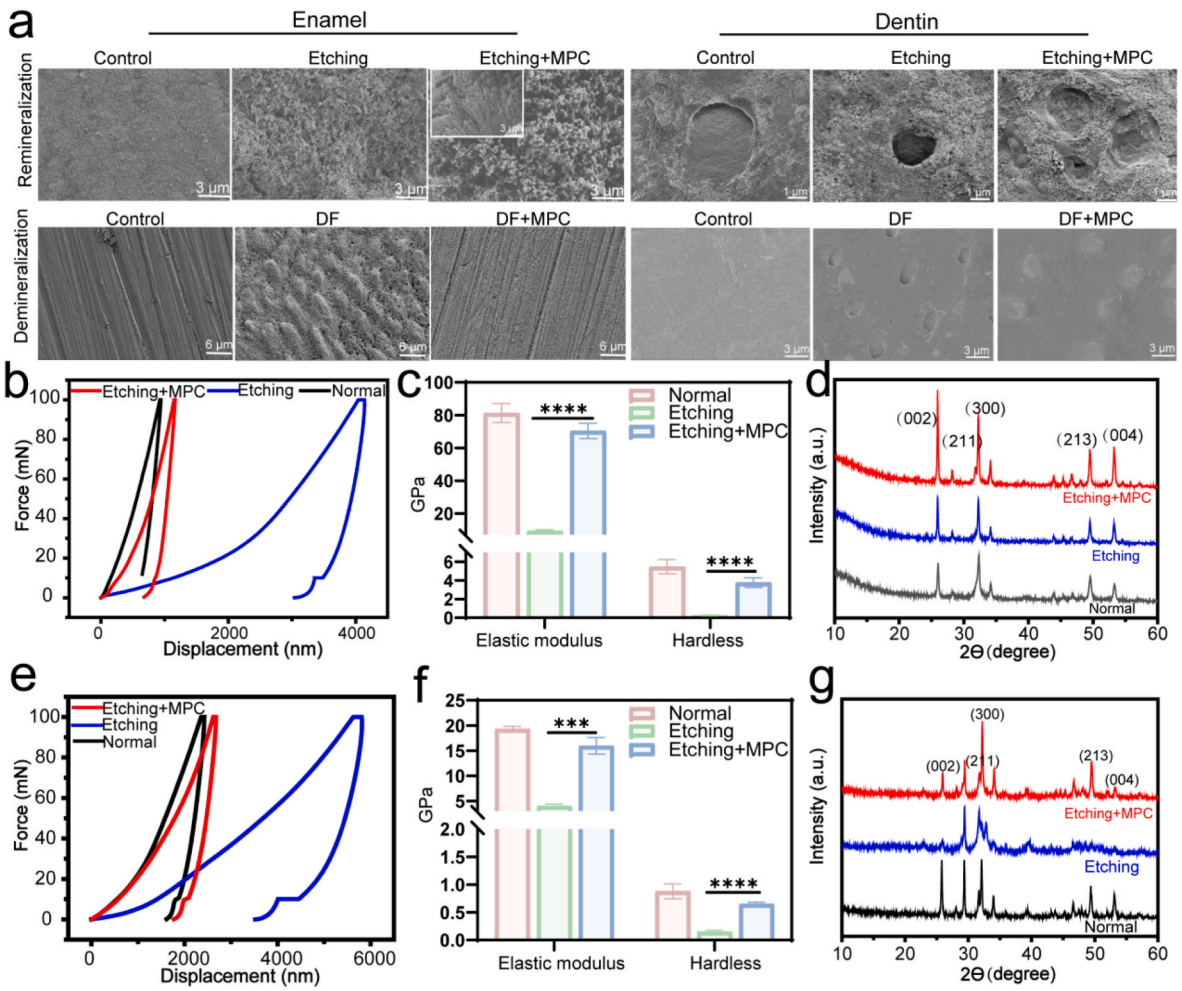

Fig. 5. The role of MPC in promoting remineralization and preventing demineralization. (a) SEM images of enamel and dentin remineralization in saliva and demineralization prevention in demineralization fluid respectively. Nanoindentation curves (b), elastic modulus, hardness (c) and XRD patterns (d) of enamel after different treatments. Nanoindentation curves (e), elastic modulus, hardness (f) and XRD patterns (g) of dentin after different treatments. Data are means ± SD. (n = 3). ***$p < 0.001$, ****$p < 0.0001$.

group was treated with MPC for 15 min every hour. 24 h later, the scale structure and rough porous surface of tooth enamel could be seen in the demineralized group, and the destruction of the structure of the enamel prisms was caused by the demineralized solution. While the enamel surface treated with MPC was smooth, and the exposure of collagen fibrils in dentin tubules was not obvious and the demineralization progression of enamel and dentin was significantly inhibited. These results suggested that gallic acid and PDA, the main components of MPC, might infiltrate into the damaged area through the enlarged pores on the enamel surface after demineralization, and attach the collagen fibers as well as demineralization crystals (such as apatite after the loss of carbonate). On the one hand, collagen could be stabilized to prevent further demineralization; on the other hand, the released Ca^{2+}, PO_4^{3-} and Mg^{2+} induced the growth and formation of new crystals outside the partially dissolved crystals.

In addition, it has been reported that Mg^{2+} can reinforce the enamel-like arrays and avoid tooth loss during the suppression of acid solubility, improving the mechanical properties of dental hard tissue [31]. To evaluate the mechanical property of the remineralized enamel and dentin treated with MPC, the nanoindentation was used to measure the microhardness and elasticity modulus. As shown in Fig. 5b–c and Fig. 5e–f, MPC could greatly restore the mechanical properties of demineralized teeth, which might be related to the dual role of MPC in mineralization promotion and released Mg^{2+} in enamel array strengthening. XRD was used to characterize the crystalline structure (Fig. 5d–g). All samples showed characteristic diffraction peaks of hydroxyapatite, and the relative intensions of different peaks after remineralization indicated that MPC had bionic remineralization effect.

3.5. Cell experiment in vitro

To evaluate the biosafety of MPC, a series of cell experiments were conducted. Firstly, staining of live and dead cells showed that MPC had no significant effect on the morphology of HOK cells, L929 cells and MC3T3-E1 cells (Fig. 6a, Fig. S20 and Fig. S21). The cytotoxicity of different samples was detected by CCK-8 assay. As shown in Fig. S22, low concentration of MPC had a certain effect of promoting proliferation of L929 cells, and with the increase of concentration, it also showed a certain negative effect on the viability of L929 cells, but still maintained over 80% activity. There was no obvious effect of MPC on HOK cells and MC3T3-E1 cells (Fig. 6b and Fig. S23). Meanwhile, the hemolysis ratios of different concentrations of MPC were less than 5% (Fig. 6c). These results proved that MPC had good biocompatibility. Here, we further explored its potential to promote osteoblast differentiation by measuring ALP activity and calcium-related mineral deposition. As shown in Fig. 6d and e, the induced ALP activity and mineralized nodules were significantly increased in the MPC group. All these results demonstrated the significant osteoinductive properties of MPC.

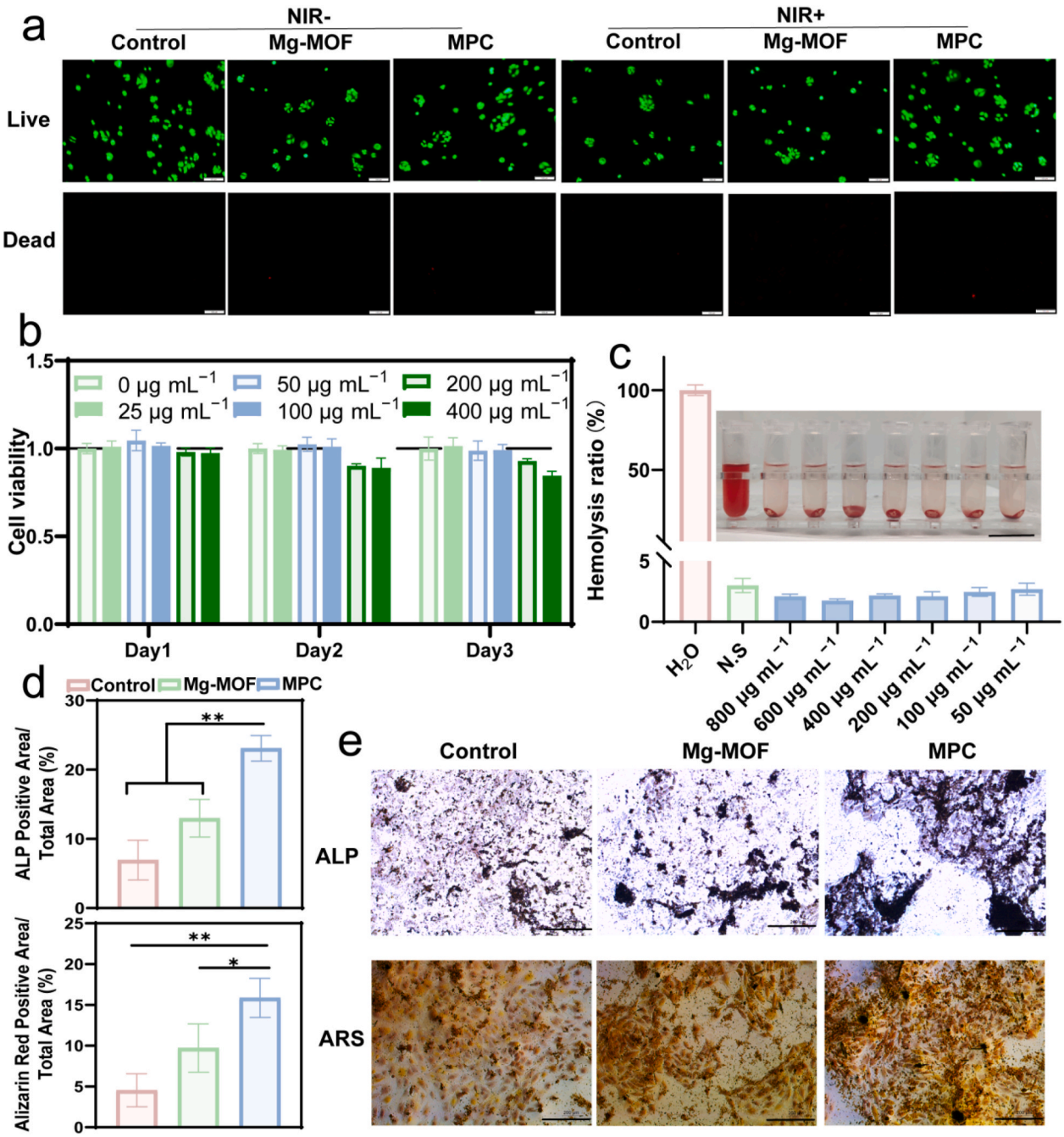

Fig. 6. Biosafety and osteogenesis potential of MPC in vitro. (a) Live and dead staining assay of HOK cells. Live and dead cells were stained with green and red fluorescent stains, respectively. (Scale bar = 100 μm). (b) Cell viabilities of HOK cells cultured with different concentrations of MPC for 1 day, 2 days and 3 days. (c) Hemolysis ratios of RBCs co-cultured with different concentrations of MPC. (Scale bar = 2 cm). (d) The proportion of ALP and alizarin red positive area. (e) The images of ALP staining and alizarin red staining. (Scale bar = 500 μm). Data are means ± SD. (n = 3). $^{*}p < 0.05$, $^{**}p < 0.01$.

3.6. *In vivo efficacy of MPC*

In order to verify the feasibility and anti-caries effect of MPC *in vivo*, we constructed the experiment on rodent model of dental caries. Firstly, the MPC was loaded with cocamidopropyl betaine (CB) to produce a non-flowing functional foam (MPC-CB), which could exist stably in braces and continue to warm up under NIR irradiation. As shown in Fig. 7a, braces containing MPC-CB foam could still uniformly heat up to approximately 49.4 °C within a short time, even with a large cooling surface. This indicated that the loaded MPC still retained its photothermal capacity, which was feasible for clinical application. Then, SD rats were treated with CB, MPC-CB and MPC-CB + NIR twice a day. After 40 days, the dental plaque biofilms were stained with 2% basic fuchsin. The processed images (Fig. S24 and Fig. 7b) showed that the dental plaque area was significantly smaller after treatment with MPC under NIR irradiation, accounting for 15.90 ± 4.09% of the total tooth area (Fig. S25). In humans, plaque area accounting for less than 20% of the tooth is considered to be basically under control [40]. Results of colony plate counting on swabs of rat first molar (Fig. 7c and Fig. S26) also demonstrated that MPC could inhibit bacterial growth and destroy biofilms with NIR irradiation.

The progression of dental caries in rats is similar to that in humans, which proceeds from shallow caries to moderate caries and deep caries with extensive lesions ultimately [2]. The anti-caries capacity of MPC

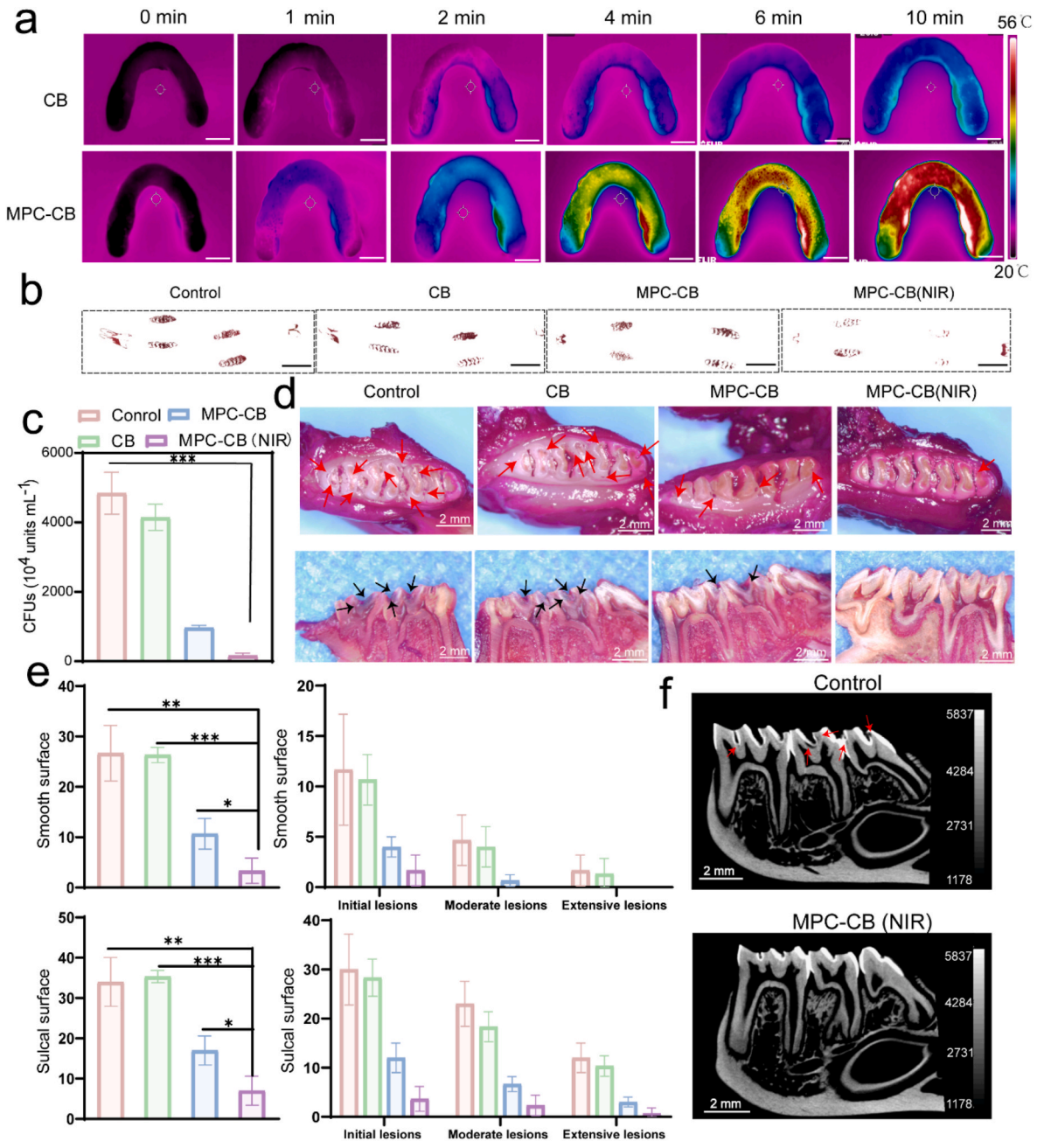

Fig. 7. Therapeutic effects of MPC on dental caries *in vivo*. (a) Thermal images of the real-time temperature of CB and MPC-CB in the mouthguard after NIR irradiation. (Scale bar = 1 cm). (b) Staining images of dental plaque in maxilla and mandible of rats. (Scale bar = 8 mm). (c) Quantitative statistics of surviving bacterial colonies in different groups. (d) Occlusal (top) and sagittal (bottom) images of rat molars under type microscope (red arrow, caries lesion sites of smooth surface; black arrow, caries lesion sites of sulcal surface). (e) Caries scores recorded from smooth surface and sulcal surface according to Larson's modification of Keyes' scoring system. (f) 2D scale sagittal images of the molars analyzed by micro-CT (red arrow, caries lesion sites). Data are means ± SD. (n = 3). *$p < 0.05$, **$p < 0.01$, ***$p < 0.001$.

under NIR irradiation was verified by analyzing the dental caries of rats. As shown in the occlusal surface (Fig. 7d, top) and sagittal image (Fig. 7d, bottom), there were more black caries and cavity lesions on the smooth surface (red arrow) and the pit (black arrow) in the Control group, while no obvious caries was observed in the MPC-CB (NIR) group. The caries scores were recorded according to Keyes' scoring system (Fig. 7e). It was evident that MPC-CB (NIR) could effectively inhibit the development of caries and completely prevent the middle and deep caries on smooth teeth, which was considered that the non-flowing properties of MPC-CB stabilized the surface of the oral microenvironment and played a synergistic antibacterial role under NIR irradiation. Due to the softness and ductility of MPC-CB, it could be retained in pit and fissure of tooth to exhibit significant inhibitory effect on caries of sulcal surface. Compared with the Control groups, the total caries of MPC-CB (NIR) was significantly reduced, and the extensive caries was almost completely suppressed regardless of smooth surface or sulcal surface. The teeth in the MPC-CB (NIR) group had a more intact volume and higher mineral density of enamel, while the Control group showed more demineralization sites (Fig. 7f, red arrow), representing the destruction of dental tissue.

Then, we further verified the *in vivo* biocompatibility of MPC-CB with NIR irradiation. Hematoxylin and eosin (H&E) staining analysis of

gingival tissue and tongue mucosa in the vicinity of the topical treatment showed no significant adverse effects of MPC-CB (NIR), such as proliferative changes, erosion, inflammatory reactions, or necrosis (Fig. S27). H&E staining of vital organs and blood routine analysis showed no abnormalities (Fig. S28 and Table S2). Blood biochemistry analyses were conducted to assess renal and liver function. Alanine aminotransferase (ALT), aspartate aminotransferase (AST) and ALP in serum were measured to assess liver function. There was no significant difference in ALT, AST and ALP between the MPC-CB (NIR) group and Control group (Fig. S29), indicating no damage to liver function. Additionally, blood urea nitrogen (BUN) and serum creatinine (CREA) were also within the normal range (Table S3), indicating no damage to kidney function. In conclusion, MPC-CB with NIR can inhibit the occurrence of extensive caries and deep caries, and has good biocompatibility.

4. Conclusion

In summary, a multifunctional MPC platform was synthesized to prevent caries and promote mineralization. The experimental results showed that the platform could respond to the danger signal (low pH value) caused by cariogenic bacteria spontaneously, and effectively removed bacterial biofilms from multiple levels of elements, genes and adhesion with NIR irradiation. While stabilizing the environmental pH value, the dissolved crystals were wrapped in the demineralization pores of the tooth surface to prevent the progress of demineralization and induced the orderly formation of new hydroxyapatite crystals. However, there are still some shortcomings in this study. First of all, the oral environment is complex, so this low pH responsive strategy may be triggered incorrectly after some acidic foods (such as carbonated drinks, fruit juices, etc.) ingestion, and more appropriate response design is needed to further refine the system. Second, the long-term safety of MPC and CB needs to be studied. Moreover, the effective use of NIR-based photothermal antibacterial in deeper areas and larger animals also needs to be further verified. Nevertheless, there are some highlights in this paper. For example, in terms of system design, this dual-responsive platform based on light control and microbial signals is used for the first time to repair dentin and enamel, which shows multi-function of bacteria killing, demineralization inhibition and mineralization promotion. In terms of system application, CB is selected as a carrier to form the non-liquid foam braces of MPC-CB, which provides a convenient operational version for new oral care materials.

Ethics approval and consent to participate

All animal procedures were performed with the Guidelines for the Care and Use of Laboratory Animals of Nanchang University in China and approved by the Animal Ethics Committee of Nanchang University (Nanchang, China, SYXK2015-0003).

All isolated teeth were extracted teeth from the patient's mouth (teeth removed during orthodontic treatment, wisdom teeth, etc.). The collection of isolated human teeth with the informed consent of patients was approved by the Medical Ethics Committee of the Affiliated Stomatological Hospital of Nanchang University. (Nanchang, China, Dental Hospital Ethics Review 2021 No. 026).

CRediT authorship contribution statement

Qun Li: Conceptualization, Methodology, Software, Writing – original draft. **Jinbiao Liu:** Data curation, Methodology. **Huijie Liu:** Investigation, Methodology. **Yue Sun:** Formal analysis, Data curation. **Yingying Xu:** Visualization, Software. **Kexin Wang:** Validation. **Wenjing Huang:** Methodology, Software. **Lan Liao:** Supervision, Funding acquisition. **Xiaolei Wang:** Validation, Project administration, Writing – review & editing, Funding acquisition.

Declaration of competing interest

All authors declared that no conflict of interest existed.

Acknowledgements

This work was funded by the National Natural Science Foundation of China (No. 31860263 to Xiaolei Wang; No. 82160194 and No. 81960492 to Lan Liao), Key Youth Project of Jiangxi Province (20202ACB216002 to Xiaolei Wang), Key Research and Development Program of Jiangxi Province (20212BBG73004 to Xiaolei Wang; 20212BBG73022 to Lan Liao), Natural Science Foundation of Jiangxi Province (No. 20181ACB20022 to Lan Liao).

Appendix B. Supplementary data

Supplementary data to this article can be found online at https://doi.org/10.1016/j.bioactmat.2023.06.017.

References

[1] Global Oral Health Status Report: towards Universal Health Coverage for Oral Health by 2030, World Health Organization, Geneva, 2022. Licence: CC BY-NC-SA 3.0 IGO.
[2] J. Zou, Q. Du, L. Ge, J. Wang, X. Wang, Y. Li, G. Song, W. Zhao, X. Chen, B. Jiang, Y. Mei, Y. Huang, S. Deng, H. Zhang, Y. Li, X. Zhou, Expert consensus on early childhood caries management, Int. J. Oral Sci. 14 (2022) 35.
[3] N. Ilie, N. Erich Serfőző, D. Prodan, J. Diegelmann, M. Moldovan, Synthesis and performance of experimental resin-based dental adhesives reinforced with functionalized graphene and hydroxyapatite fillers, Mater. Des. 221 (2022), 110985.
[4] B.M. Oosterlaken, M.P. Vena, G. de, With, *In vitro* mineralization of collagen, Adv. Mater. 33 (2021), e2004418.
[5] Q. Wang, J. Luan, Z. Zhao, W. Kong, C. Zhang, J. Ding, Dentin-desensitizing biomaterials, Chin. Chem. Lett. 14 (2022), 108060.
[6] L. Tanner, D. Craig, R. Holmes, L. Catinella, P. Moynihan, Does dental caries increase risk of undernutrition in children? JDR Clinic. Translation. Res. 7 (2021) 104–117.
[7] Q. Li, J. Liu, Y. Xu, H. Liu, J. Zhang, Y. Wang, Y. Sun, M. Zhao, L. Liao, X. Wang, Fast cross-linked hydrogel as a green light-activated photocatalyst for localized biofilm disruption and brush-free tooth whitening, ACS Appl. Mater. Interfaces 14 (2022) 28427–28438.
[8] J. Jin, Screening and interventions to prevent dental caries in young children, JAMA 326 (2021) 2223.
[9] L. Weng, L. Wu, R. Guo, J. Ye, W. Liang, W. Wu, L. Chen, D. Yang, Lactobacillus cell envelope-coated nanoparticles for antibiotic delivery against cariogenic biofilm and dental caries, J. Nanobiotechnol. 20 (2022) 356.
[10] K. Lewis, The science of antibiotic discovery, Cell 181 (2020) 29–45.
[11] D. Liu, X. Ma, Y. Ji, R. Chen, S. Zhou, H. Yao, Z. Zhang, M. Ye, Z. Xu, M. Du, Bioresponsive nanotherapy for preventing dental caries by inhibiting multispecies cariogenic biofilms, Bioact. Mater. 14 (2021) 1–14.
[12] J. He, J. Yang, M. Li, Y. Li, Y. Pang, J. Deng, X. Zhang, W. Liu, Polyzwitterion manipulates remineralization and antibiofilm functions against dental demineralization, ACS Nano 16 (2022) 3119–3134.
[13] M. Fan, M. Li, Y. Yang, M.D. Weir, Y. Liu, X. Zhou, K. Liang, J. Li, H.H.K. Xu, Dual-functional adhesive containing amorphous calcium phosphate nanoparticles and dimethylaminohexadecyl methacrylate promoted enamel remineralization in a biofilm-challenged environment, Dent. Mater. 38 (2022) 1518–1531.
[14] L. Zhang, Q.-L. Li, H.M. Wong, Evaporation strategy generated antibacterial enamel-like fluorapatite-polyacrylic acid sheet for functional dental restoration, Compos. B Eng. 233 (2022), 109651.
[15] T. Thyvalikakath, M. LaPradd, Z. Siddiqui, W.D. Duncan, G. Eckert, J.K. Medam, D. B. Rindal, M. Jurkovich, G.H. Gilbert, Root canal treatment survival analysis in national dental PBRN practices, J. Dent. Res. 101 (2022) 1328–1334.
[16] Y. Xu, Y. You, L. Yi, X. Wu, Y. Zhao, J. Yu, H. Liu, Y. Shen, J. Guo, C. Huang, Dental plaque-inspired versatile nanosystem for caries prevention and tooth restoration, Bioact. Mater. 20 (2022) 418–433.
[17] M.R. Passos, R.S. Almeida, B.O. Lima, J.Z.d.S. Rodrigues, N.S.d. Macêdo Neres, L. S. Pita, P.D.O.F. Marinho, I.A. Santos, J.P. da Silva, M.C. Oliveira, M.A. Oliveira, S. M.B. Pessoa, M.M.L. Silva, P.H.S. Silveira, M.M. Reis, I.P. Santos, L.d.O.N. Ricardo, L.O.S.B. Andrade, A.B. Soares, T.M.L. Correia, É.P.d. Souza, P.N. Pires, M.P. Cruz, L.M. Marques, A.P.T. Uetanabaro, R. Yatsuda, Anticariogenic activities of Libidibia ferrea, gallic acid and ethyl gallate against Streptococcus mutans in biofilm model, J. Ethnopharmacol. 274 (2021), 114059.
[18] H. Wang, M.I. Fowler, D.J. Messenger, J.J. Ordaz-Ortiz, X. Gu, S. Shi, L.A. Terry, M. J. Berry, G. Lian, S. Wang, Inhibition of the intestinal postprandial glucose transport by gallic acid and gallic acid derivatives, Food Funct. 12 (2021), 5399–5406.
[19] Y. Wang, J. Zhou, L. Yuan, F. Wu, L. Xie, X. Yan, H. Li, Y. Li, L. Shi, R. Hu, Y. Liu, Neighboring carboxylic acid boosts peroxidase-like property of metal-phenolic

nano-networks in eradicating Streptococcus mutans biofilms, 19 (2023) 2206657, Small 19 (2022), 2206657.
[20] Y. Zhan, X. Hu, Y. Li, Y. Wang, H. Chen, C.A. Omolo, T. Govender, H. Li, F. Huang, L. Shi, X. Hu, Y. Liu, Antimicrobial hybrid amphiphile via dynamic covalent bonds enables bacterial biofilm dispersal and bacteria eradication, Adv. Funct. Mater. 30 (2020), 2000537.
[21] M. Qi, X. Ren, W. Li, Y. Sun, X. Sun, C. Li, S. Yu, L. Xu, Y. Zhou, S. Song, B. Dong, L. Wang, NIR responsive nitric oxide nanogenerator for enhanced biofilm eradication and inflammation immunotherapy against periodontal diseases, Nano Today 43 (2022), 101447.
[22] K. Cheng, P. She, H. Wang, Z. Wang, L. Zhang, X. Tang, L. Yuan, Y. Feng, X. Song, G. Pan, J. Yang, L. Liu, A bio-inspired versatile free-standing membrane for oral cavity microenvironmental monitoring and remineralization to prevent dental caries, Mater. Horiz. 10 (2023) 512–523.
[23] X. Shi, W. Liu, Y. Xu, C. Jin, G. Zhang, Y. Shi, H. Huang, J. Sun, J. Yang, Ultraviolet-selective organic phototransistors for low-power skin-inspired nociceptor, Nano Energy 110 (2023), 108372.
[24] H. Guo, X. Zhang, Z. Chen, L. Zhang, L. Wang, J. Xu, M. Wu, High-energy short-wave blue light conversion films via carbon quantum dots for preventing retinal photochemical damage, Carbon 199 (2022) 431–438.
[25] M. Yin, J. Wu, M. Deng, P. Wang, G. Ji, M. Wang, C. Zhou, N.T. Blum, W. Zhang, H. Shi, N. Jia, X. Wang, P. Huang, Multifunctional magnesium organic framework-based microneedle patch for accelerating diabetic wound healing, ACS Nano 15 (2021) 17842–17853.
[26] J. Hu, Y. Ding, B. Tao, Z. Yuan, Y. Yang, K. Xu, X. Li, P. Liu, K. Cai, Surface modification of titanium substrate *via* combining photothermal therapy and quorum-sensing-inhibition strategy for improving osseointegration and treating biofilm-associated bacterial infection, Bioact. Mater. 18 (2022) 228–241.
[27] J. Yu, H. Bian, Y. Zhao, J. Guo, C. Yao, H. Liu, Y. Shen, H. Yang, C. Huang, Epigallocatechin-3-gallate/mineralization precursors co-delivery hollow mesoporous nanosystem for synergistic manipulation of dentin exposure, Bioact. Mater. 23 (2022) 394–408.
[28] L. Wu, Q. Wang, Y. Li, M. Yang, M. Dong, X. He, S. Zheng, C.Y. Cao, Z. Zhou, Y. Zhao, Q. Li, A dopamine acrylamide molecule for promoting collagen biomimetic mineralization and regulating crystal growth direction, ACS Appl. Mater. Interfaces 13 (2021) 39142–39156.
[29] C.S. Kovacs, C. Chaussain, P. Osdoby, M.L. Brandi, B. Clarke, R.V. Thakker, The role of biomineralization in disorders of skeletal development and tooth formation, Nat. Rev. Endocrinol. 17 (2021) 336–349.
[30] S. Tang, Z. Dong, X. Ke, J. Luo, J. Li, Advances in biomineralization-inspired materials for hard tissue repair, Int. J. Oral Sci. 13 (2021) 42.
[31] Y. Li, Y. Kong, B. Xue, J. Dai, G. Sha, H. Ping, L. Lei, W. Wang, K. Wang, Z. Fu, Mechanically reinforced artificial enamel by Mg^{2+}-induced amorphous intergranular phases, ACS Nano 16 (2022) 10422–10430.
[32] Z. Zheng, Y. Chen, B. Guo, Y. Wang, W. Liu, J. Sun, X. Wang, Magnesium-organic framework-based stimuli-responsive systems that optimize the bone microenvironment for enhanced bone regeneration, Chem. Eng. J. 396 (2020), 125241.
[33] S. Zhang, B. Mao, S. Cui, Q. Zhang, J. Zhao, X. Tang, W. Chen, Absorption, metabolism, bioactivity, and biotransformation of epigallocatechin gallate, Crit. Rev. Food Sci. Nutr. (2023) 1–21.
[34] Y. Qin, G. Lin, W. Chen, X. Xu, Q. Yan, Flagellar motility is necessary for Aeromonas hydrophila adhesion, Microb. Pathog. 98 (2016) 160.
[35] J. Wu, P. Shen, X. Qin, Y. Yang, C. Lin, X. Li, W. Geng, P. Gao, L. Chen, L. Miao, Y. Jiao, B. Tao, Self-supply of H_2O_2 and O_2 by a composite nanogenerator for chemodynamic therapy/hypoxia improvement and rapid therapy of biofilm-infected wounds, Chem. Eng. J. 459 (2023), 141507.
[36] K. Sauer, P. Stoodley, D.M. Goeres, L. Hall-Stoodley, M. Burmølle, P.S. Stewart, T. Bjarnsholt, The biofilm life cycle: expanding the conceptual model of biofilm formation, Nat. Rev. Microbiol. 20 (2022) 608–620.
[37] Y. Deng, Y. Yang, B. Zhang, H. Chen, Y. Lu, S. Ren, L. Lei, T. Hu, The vicK gene of *Streptococcus mutans* mediates its cariogenicity *via* exopolysaccharides metabolism, Int. J. Oral Sci. 13 (2021) 45.
[38] P. Yu, F. Yu, J. Xiang, K. Zhou, L. Zhou, Z. Zhang, X. Rong, Z. Ding, J. Wu, W. Li, Z. Zhou, L. Ye, W. Yang, Mechanistically scoping cell-free and cell-dependent artificial scaffolds in rebuilding skeletal and dental hard tissues, Adv. Mater. 34 (2021), e2107922.
[39] S. Tao, J. Yang, Z. Su, F. Zhou, Z. Wang, Y. Yang, L. Sun, Y. Deng, K. Liang, J. Li, A dentin biomimetic remineralization material with an ability to stabilize collagen, Small 18 (2022), e2203644.
[40] P. Marsh, Microbiology of dental plaque biofilms and their role in oral health and caries, Chem. Soc. Rev. 54 (2010) 441–454.